Journal of Solid State Chemistry 182 (2009) 1631–1637

Contents lists available at ScienceDirect

Journal of Solid State Chemistry

journal homepage: www.elsevier.com/locate/jssc

Mesoporous hybrids containing Eu^{3+} complexes covalently bonded to SBA-15 functionalized: Assembly, characterization and photoluminescence

Li Li Kong, Bing Yan *, Ying Li

Department of Chemistry, Tongji University, Siping Road 1239, Shanghai 200092, China

ARTICLE INFO

Article history:
Received 20 January 2009
Received in revised form
25 March 2009
Accepted 29 March 2009
Available online 14 April 2009

Keywords:
Mesoporous hybrid materials
Lanthanide complex
Luminescence

ABSTRACT

A novel series of luminescent mesoporous organic–inorganic hybrid materials has been prepared by linking Eu^{3+} complexes to the functionalized ordered mesoporous SBA-15 which was synthesis by a co-condensation process of 1,3-diphenyl-1,3-propanepione (DBM) modified by the coupling agent 3-(triethoxysilyl)-propyl isocyanate (TEPIC), tetraethoxysilane (TEOS), Pluronic P123 surfactant as a template. It was demonstrated that the efficient intramolecular energy transfer in the mesoporous material Eu(DBMSi-SBA-15)$_3$phen mainly occurred between the modified DBM (named as DBM-Si) and the central Eu^{3+} ion. So the Eu(DBMSi-SBA-15)$_3$phen showed characteristic emission of Eu^{3+} ion under UV irradiation with higher luminescence quantum efficiency. Moreover, the mesoporous hybrid materials exhibited excellent thermal stability as the lanthanide complex was covalently bonded to the mesoporous matrix.

1. Introduction

It is well known that RE complexes can give sharp, intense emission lines upon ultraviolet light irradiation, because of the effective intramolecular energy transfer from the coordinated ligands to the luminescent central lanthanide ion, which in turn undergoes the corresponding radiative emitting process (i.e., "antenna effect") [1]. Some of the RE complexes have potential applications in efficient light-conversion molecular devices and organic light-emitting devices [2–5]. But, their practical applications have been restricted owing to the inherent disadvantages, such as low chemical, optical, and thermal stabilities. Recently, the luminescence properties of RE complexes supported on a solid matrix were studied extensively because their photophysical properties could be modified by interaction of the host structure [6–9]. Lanthanide complexes incorporated into inorganic or organic/inorganic matrices by low-temperature soft-chemistry process, including the sol–gel method and hydrothermal synthesis process can effectively overcome the disadvantages discussed above. The hybrid materials enable both inorganic and organic dopants to be incorporated with relatively high thermal stability [10–12]. Many investigations were carried out on doping the inorganic silica materials with the lanthanide complexes in which only weak physical interactions exist between these two phases, such as van der Waals force, hydrogen bonding, or weak static effect [13–15]. Besides, this method cannot control the clustering of emitting centers which lead to inhomogeneous dispersion and leaching of the photoactive molecules in the materials. Our research group concentrated on covalently grafting the ligand to the inorganic networks. By using different modified routes, including the modification of active amino group, hydroxyl groups, and carboxyl groups with coupling agent, etc., we synthesized different materials in which lanthanide complexes luminescent centers were bonded with siloxane matrix through Si–C linkage [16–18].

Mesostructured and mesoporous materials are emerging as a new class of optical materials, especially as a special type of nanomaterials with ordered arrays of uniform nanochannels. And the mesoporous molecular sieves used as a support for RE complexes have attracted particular attention [19–21]. There are two typical mesoporous molecular sieves materials used as support: M41S and SBA-15. Lanthanide tris- and tetrakis-β-diketonates have been immobilized in the mesoporous silicas MCM-41 and MCM-48 by simple wet impregnation method [22]. SBA-15 is a typical mesoporous material with largest pore-size mesochannels, thick walls, adjustable pore size from 3 to 30 nm, and high hydrothermal, thermal, mechanical stability. Some work focus on using it as host for incorporation of active molecules have been reported [23–25]. The large number of hydroxyl in SBA-15 provides necessary qualification for the modification of inner face and self assembly of huge guest molecules, namely, providing outstanding hosts for self aggregation chemistry. Recently, some work concerning on preparing the organic/inorganic hybrids through functionalization of the exterior and/or interior surfaces made the mesoporous SBA-15 have more extensive applications. Our research team has reported the synthesis and luminescence

* Corresponding author. Fax: +86 21 65982287.
E-mail address: byan@tongji.edu.cn (B. Yan).

0022-4596/$ - see front matter © 2009 Elsevier Inc. All rights reserved.
doi:10.1016/j.jssc.2009.03.036

properties of SBA-15 mesoporous materials covalently bonded with lanthanide complexes.

In this paper, we synthesized SBA-15 mesoporous hybrid material functionalized by 1,3-diphenyl-1,3-propanepione (DBM) (DBMSi-SBA-15), in which DBM was covalently bonded to the framework of SBA-15 by co-condensation of the modified DBM (denoted as DBM-Si) and the tetraethoxysilane (TEOS) using the Pluronic P123 surfactant as template. By introducing $Eu(NO_3)_3$ and 1,10-phenanthroline (phen) complex into the hybrid material via a ligand exchange reaction, we obtained the highly luminescent ternary complex $Eu(DBMSi)_3phen$ functionalized SBA-15, denoted as $Eu(DBMSi\text{-}SBA\text{-}15)_3phen$. And we also demonstrated that the ternary europium complex $Eu(DBMSi)_3phen$ was successfully linked to the framework of SBA-15 by a covalently bonded DBM group. Furthermore, we synthesized the pure $Eu(DBMSi)_3$-phen complex for comparison. The photoluminescence properties of all these materials were investigated in detail.

2. Experimental section

2.1. Chemicals

Pluronic P123 (EO20PO70EO20) and tetraethoxysilane were purchased from Aldrich. 3-(triethoxysiyl)-propyl isocyanate (TEPIC) was supplied by Lancaster. The solvent tetrahydrofuran (THF) was used after desiccation with anhydrous calcium chloride. Europium nitrate [$Eu(NO_3)_3$] was obtained by dissolving Eu_2O_3 in concentrated nitric acid (HNO_3).

2.2. Synthesis

2.2.1. Synthesis of DBM-functionalized SBA-15 mesoporous material (denoted as DBMSi-SBA-15)

The modified precursor DBM-Si was prepared according to the procedure reported in the literature, described as follows: Firstly, 1,3-diphenyl-1,3-propanepione (1 mmol, 0.2243 g) was dissolved in 20 mL of dehydrated tetrahydrofuran, and then NaH (2 mmol, 0.048 g) was added into the solution with incessant stirring. Two hours later, 2.2 mmol (0.5442 g) of 3-(triethoxysilyl)-propyl-isocyanate was dropwise added into the refluxing solution. Then the mixture was heated at 65 °C in a covered flask for 12 h at the nitrogen atmosphere. A yellow oil sample i.e. the precursor DBM-Si was furnished after isolation and purification. The mesoporous material DBMSi-SBA-15 was synthesized from acidic mixture with the following molar composition: 0.0172 P123: 0.96 TEOS: 0.04 DBM-Si: 6 HCl: 208.33 H_2O. P123 (1.0 g) was firstly dissolved in the deionized water (7.5 g) and 2 M HCl solution (30 g) at room temperature. After that the mixture of DBM-Si and TEOS was added into the above solution followed by 24 h of persistent stirring. Then it was heated at 100 °C for 48 h in a Teflon bottle sealed in an autoclave. The solid product was filtered and washed thoroughly with deionized water, and dried at 60 °C. The ethanol was used to remove the copolymer surfactant P123 via Soxhlet extraction method under reflux for 2 days. After drying in vacuum the material showed a light-yellow color.

2.2.2. Synthesis of SBA-15 mesoporous material covalently bonded with the Eu^{3+} complex (denoted as $Eu(DBMSi\text{-}SBA\text{-}15)_3phen$)

The DBMSi-SBA-15 derived hybrid mesoporous material containing Eu^{3+} was prepared as follows: DBMSi-SBA-15 was soaked in an appropriate amount of $Eu(NO_3)_3$ and 1,10-phenanthroline (phen) ethanol solution with stirring, the molar ratio of Eu^{3+}:DBM-Si:phen is 1:3:1. After being stirred for 12 h at room temperature, the mixture was filtrated and washed with EtOH.

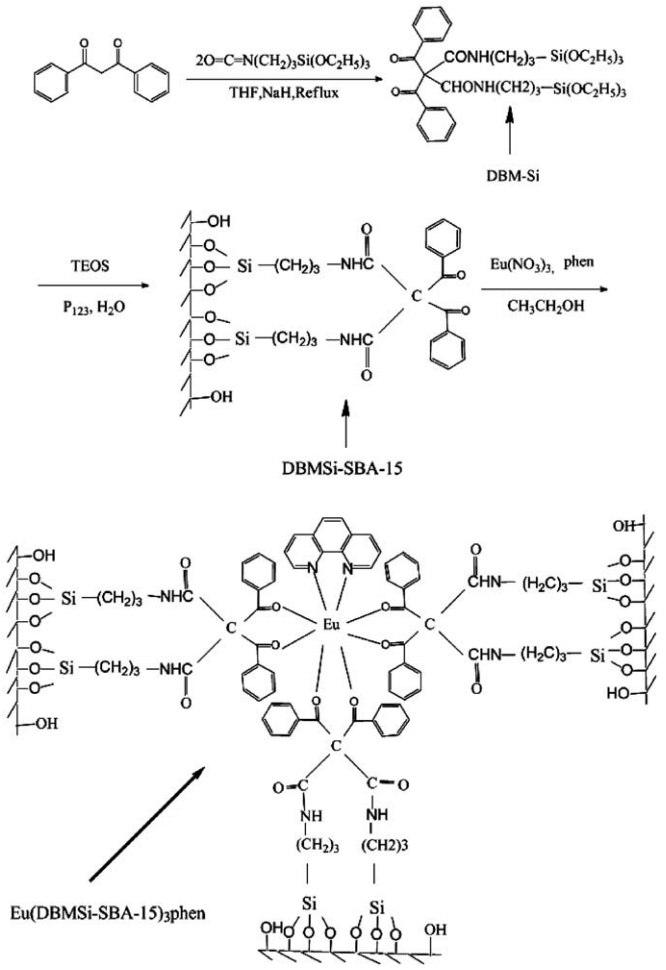

Fig. 1. Scheme of the synthesis process of DBM-Si and predicted structure of hybrid mesoporous material $Eu(DBMSi\text{-}SBA\text{-}15)_3phen$.

Finally the material was dried at 60 °C under vacuum overnight, denoted as $Eu(DBMSi\text{-}SBA\text{-}15)_3phen$. The predicted structure of $Eu(DBMSi\text{-}SBA\text{-}15)_3phen$ was shown in Fig. 1. The modified ligand was covalently bonded to the SBA-15 host through Si–O–Si by the hydrolysis–condensation of organic functionality DBM-Si.

2.2.3. Synthesis of SBA-15 mesoporous material covalently bonded with the binary Eu^{3+} complex (denoted as $Eu(DBMSi\text{-}SBA\text{-}15)_3$)

The synthesis procedure for $Eu(DBMSi\text{-}SBA\text{-}15)_3$ was similar to that of $Eu(DBMSi\text{-}SBA\text{-}15)_3phen$ except that $Eu(NO_3)_3$ replace the mixed ethanol solution of $Eu(NO_3)_3$ and phen.

2.2.4. Characterization

IR spectra were measured within the 4000–400 cm^{-1} region on an infrared spectrophotometer with the KBr pellet technique. The ultraviolet absorption spectra were taken with an Agilent 8453 spectrophotometer (CCl_4 solution). X-ray powder diffraction patterns were recorded on a Rigaku D/max-rB diffractometer equipped with a Cu anode in a 2θ range from 0.6° to 6°. Nitrogen adsorption/desorption isotherms were measured at the liquid nitrogen temperature, using a Nova 1000 analyzer. Before the measurements, the sample were outgassed for 2 h in the degas port of the adsorption apparatus at 423 K. Surface areas were calculated by the Brunauer–Emmett–Teller (BET) method and pore size distributions were evaluated from the desorption branches of the nitrogen isotherms using the Barrett–Joyner–Halenda (BJH) model. Transmission electron microscope (TEM)

experiments were conducted on a JEOL2011 microscope operated at 200 kV. Thermogravimetric analysis (TGA) was performed on a Netzsch STA 409 at a heating rate of 10 °C/min under nitrogen atmosphere. The fluorescence excitation and emission spectra were obtained on RF-5301 spectrophotometer. All spectra are normalized to a constant intensity at the maximum. Luminescence lifetime measurements were carried out on an Edinburgh FLS920 phosphorimeter using a 450 W xenon lamp as excitation source.

3. Results and discussion

3.1. DBM-functionalized mesoporous silica SBA-15

Fig. 2 shows the UV absorption spectra of DBM (A), DBM-Si (B). Comparing the absorption spectrum of DBM-Si (B) with that of DBM (A), the absorption band corresponded to the $\pi \rightarrow \pi^*$ electronic transition locate at different wavelength. There was a blue shift from 342 to 334 nm. The blue shift indicates the DBM was successfully grafted by 3-(triethoxysilyl)-propyl isocyanate because the modifications influence the energy difference levels among electron transitions.

The IR spectra of the DBM (A), DBM-Si (B) and Eu(DBMSi-SBA-15)$_3$ (C) are showed in Fig. 3. Comparing the spectra of DBM(A) and DBM-Si(B), the vibration of –CH_2– at 3059 cm^{-1} (A) was taken place by a strong broad band located at 2963 cm^{-1} (B), which designates the three methylene groups of 3-(triethoxysilyl)-propyl isocyanate. Besides, in Fig. 3(B) the band centered at 3351 cm^{-1} corresponds to the stretching vibration of grafted –NH– groups. Moreover, the spectrum of DBM-Si is dominated by ν(C–Si, 1164 cm^{-1}) and ν(Si–O, 1083 cm^{-1}) absorption bands, characteristic of trialkoxylsilyl functions. In addition, the bending vibration (δ_{NH}, 1552 cm^{-1}) is another evidence of the formation of amide groups. New bands at 1778 and 1704 cm^{-1} derived from the $C{=}O$ absorptions of TEPIC proved that 3-(triethoxysilyl)-propyl isocyanate was successfully grafted onto the –CH_2– groups of the coupling agent. In the IR spectra of Eu(DBMSi-SBA-15)$_3$ Fig. 2C, the bands located at 1075 cm^{-1} (ν_{as}, Si–O), 805 cm^{-1} (ν_s, Si–O), and 457 cm^{-1}(δ, Si–O–Si) (ν represents stretching, δ in plane bending, s symmetric, and as asymmetric vibrations) can show the formation of the Si–O–Si framework. Furthermore, the band at 1640 cm^{-1} which are originating from –CONH– group of DBM-Si in hybrid mesoporous material Eu(DBMSi-SBA-15)$_3$ (C) is consistent with the fact that the DBM group in the framework remains intact even after both hydrolysis–condensation reaction and the surfactant extraction procedure [26].

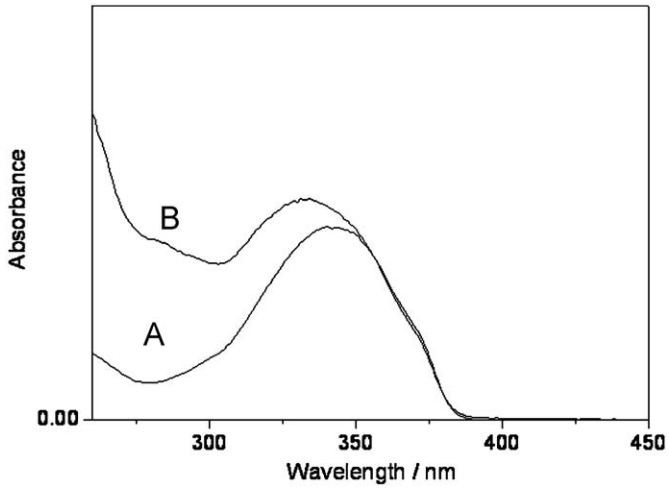

Fig. 2. UV absorption spectra for DBM (A) and DBM-Si (B).

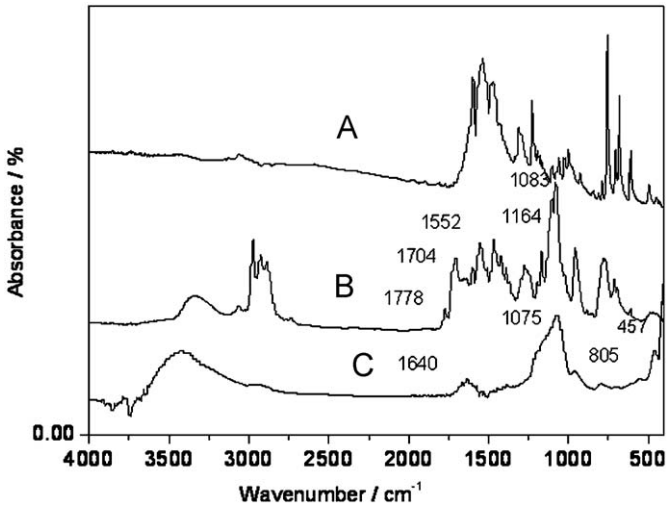

Fig. 3. IR spectra for DBM (A), DBM-Si (B), and Eu(DBMSi-SBA-15)$_3$ (C).

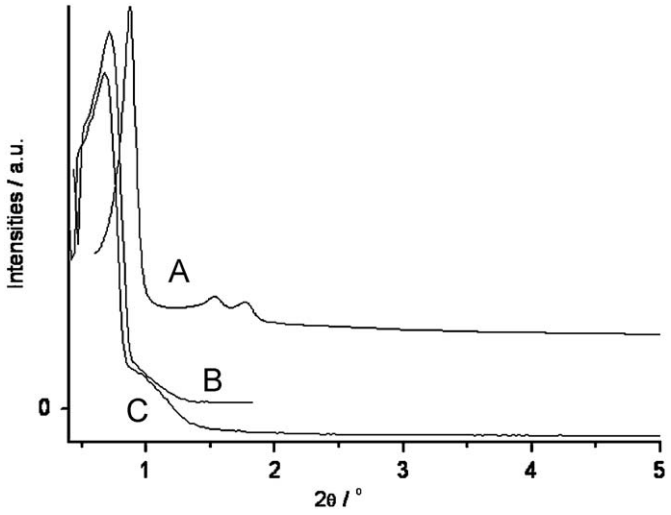

Fig. 4. SAXRD patterns of SBA-15 (A), Eu(DBMSi-SBA-15)$_3$ (B) and Eu(DBMSi-SBA-15)$_3$phen (C).

3.2. Europium (Eu^{3+}) complexes covalently bonded to DBM-functionalized mesoporous SBA-15

SBA-15 is a kind of highly ordered mesoporous material with hexagonal symmetry of the space group *p6mm*. These characters can be proved by the small-angle X-ray diffraction (SAXRD) patterns and nitrogen adsorption/desorption isotherms. Fig. 4 shows the SAXRD patterns of a pure SBA-15 mesporous silicon (A), Eu(DBMSi-SBA-15)$_3$ (B) and Eu(DBMSi-SBA-15)$_3$phen(C). It is obvious that the SBA-15 mesporous materials exhibit three well-resolved diffraction peaks that can be indexed as (100), (110), and (200) reflections associated with 2-D hexagonal symmetry (*p6mm*), confirming a well-ordered mesoporous structure in the samples. But the XRD patterns for Eu(DBMSi-SBA-15)$_3$ (B) and Eu(DBMSi-SBA-15)$_3$phen (C) did not feature clear (110) and (200) reflections. It is because that the hybrid mesoporous material has a lower degree of order as the introduction of the Eu^{3+} compared with the pure SBA-15. In the pattern of Eu^{3+} complexes

functionalized mesoporous materials the intensity of these characteristic diffraction peaks slightly decreased, which is probably attributed to the presence of guest moieties onto the mesoporous framework of SBA-15, resulting in the decrease of crystallinity, but not the collapse in the pore structure of mesoporous materials [27].

Fig. 5 shows the N_2 adsorption–desorption isotherm of the pure SBA-15 (A), Eu(DBMSi-SBA-15)$_3$ (B), and Eu(DBMSi-SBA-15)$_3$phen (C). They all display typical IV isotherms with clear H1-type hysteresis loops at high relative pressure according to the IUPAC classification [28], characteristic of mesoporous materials with highly uniform size distributions. This phenomenon indicated that the typical SBA-15 mesoporous material was obtained. From the two branches of adsorption–desorption isotherms, it can be observed that there is a sharp adsorption step in the P/P_0 region from 0.6 to 0.8 and a hysteresis loop at the relative pressure $P/P_0 > 0.7$, which shows that the materials process a well defined array of regular mesopores. The textural data of the materials are given in Table 1. The specific area and the pore size have been calculated by using Brunauer–Emmett–Teller and Barrett–Joyner–Halenda methods, respectively. These data show both Eu(DBMSi-SBA-15)$_3$ and Eu(DBMSi-SBA-15)$_3$phen exhibit a smaller specific area, a slightly smaller pore size and a pore volume compared with pure SBA-15, which might be due to the presence of organic ligand DBM on the pore surface and the co-surfactant effect of DBM-Si. The co-surfactant effect which means the interaction between DBM-Si and surfactant reduces the diameter of the micelles [29]. Furthermore, this is the evidence of that the Eu^{3+} complexes was incorporated in the channels of SBA-15.

TEM image of Eu(DBMSi-SBA-15)$_3$phen is presented in Fig. 6. From the TEM images, we could find that the ordered mesostructure was still substantially conserved after the introducing of

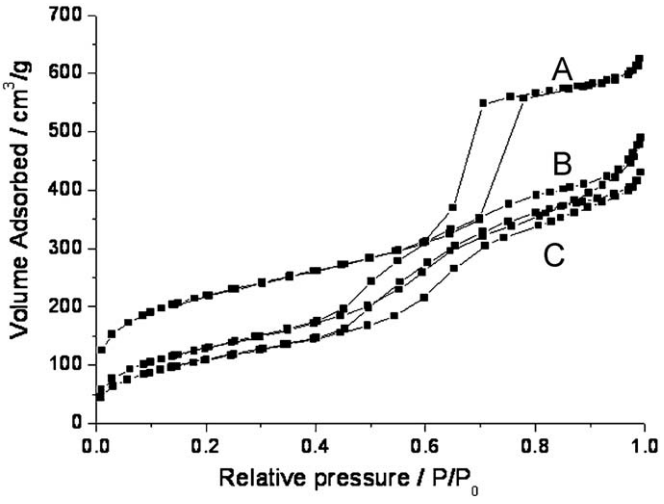

Fig. 5. N_2 adsorption/desorption isotherms of pure SBA-15 (A), Eu(DBMSi-SBA-15)$_3$ (B), and Eu(DBMSi-SBA-15)$_3$phen (C).

Table 1
Textural data of SBA-15, Eu(DBMSi-SBA-15)$_3$ and Eu(DBMSi-SBA-15)$_3$phen.

Sample	S_{BET} (m^2/g)	V (cm^3/g)	D_{BJH} (nm)
SBA-15	746	0.97	5.64
Eu(DBMSi-SBA-15)$_3$	475	0.75	5.37
Eu(DBMSi-SBA-15)$_3$phen	427	0.68	5.51

S_{BET}—the BET surface area; V—the pore volume; and D—the pore diameter.

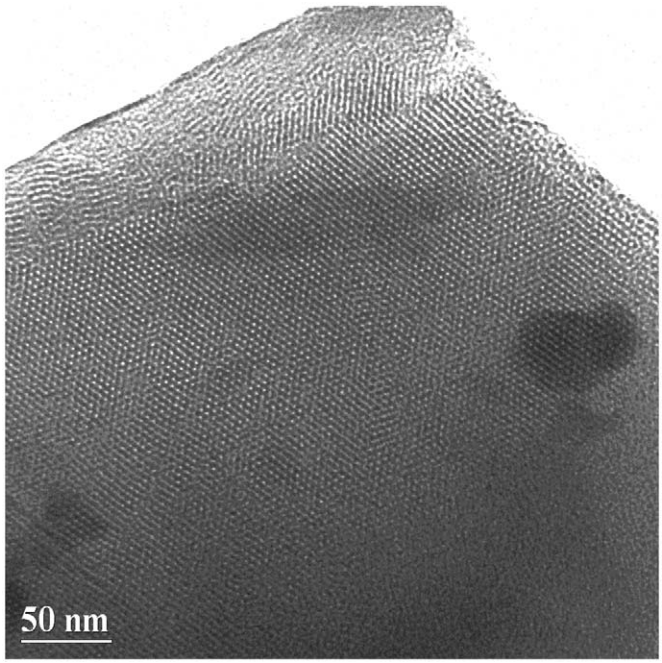

Fig. 6. TEM image of Eu(DBMSi-SBA-15)$_3$phen.

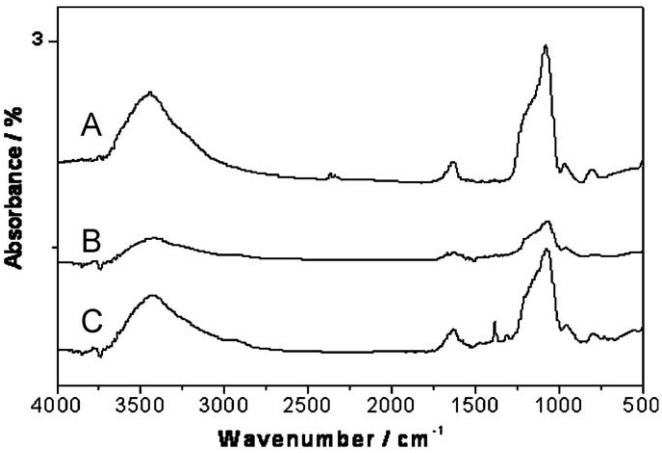

Fig. 7. IR spectra of SBA-15 (A), Eu(DBMSi-SBA-15)$_3$ (B), and Eu(DBMSi-SBA-15)$_3$phen (C).

Eu^{3+}. The hexagonal symmetry of Eu(DBMSi-SBA-15)$_3$phen inferred from XRD is in accord with the TEM investigation.

The IR spectra of SBA-15 (A), Eu(DBMSi-SBA-15)$_3$ (B) and Eu(DBMSi-SBA-15)$_3$phen (C) are shown in Fig. 7. In the spectrum of SBA-15 material (A), the band appearing at 1082 cm^{-1} is corresponds to asymmetric Si–O stretching vibration modes (ν_{as}, Si–O), and the band at 796 cm^{-1} can be attributed to the symmetric Si–O stretching vibration (ν_s, Si–O). The bands attributed to Si–O–Si bending vibration (δ, Si–O–Si), and the silanol (Si–OH) stretching vibrations of surface groups located at 457 and 968 cm^{-1}, respectively [30]. The band appearing at 3449 cm^{-1} is the evidence of the presence of hydroxyl. All the hybrid mesoporous materials exhibit the similar infrared absorption bands, which consistent with the characters of the silica framework. Furthermore, the bands at 1380–1555 cm^{-1} range appearing in the spectra of Eu(DBMSi-SBA-15)$_3$ and Eu(DBMSi-SBA-15)$_3$phen is originated from the –CONH– group of DBM-Si, suggesting that DBM-Si has been successfully grafted onto the wall of SBA-15.

3.3. Thermogravimetric analysis

The thermogravimetric weight loss curve of Eu(DBMSi-SBA-15)$_3$phen (A) and pure complex Eu(DBMSi)$_3$phen (B) were given in Fig. 8. From A to B, it can be observed that the mesoporous materials have remained the more residual mass (75%) compared to the pure complex Eu(DBMSi)$_3$phen (55%). Furthermore, the TGA curve of mesoporous materials Eu(DBMSi-SBA-15)$_3$phen has one decomposition platform while the pure complex Eu(DBMSi)$_3$phen has two decomposition stages, indicating that the mesoporous materials is more stable for thermal treatment compared to the pure complex. The TGA curve of Eu(DBMSi-SBA-15)$_3$phen shows a large mass decrease (18%) in heat flow around 381 °C, which is attributed to the loss of the thermal degradation of the mesoporous material framework, involving Si–C, C–C, and C–N bond cleavage seen from Fig. 8A, and the TGA curve of Eu(DBMSi)$_3$phen shows two decreases, namely, mass changes of 13% and 14% around 255 and 345 °C, which are attributable to the loss of the ligand DBM and the thermal degradation of the mesoporous material framework (as shown in Fig. 8B). All the phenomena illustrated that the thermal stability of the pure complex was enhanced when it was covalently bonded to the mesoporous matrix.

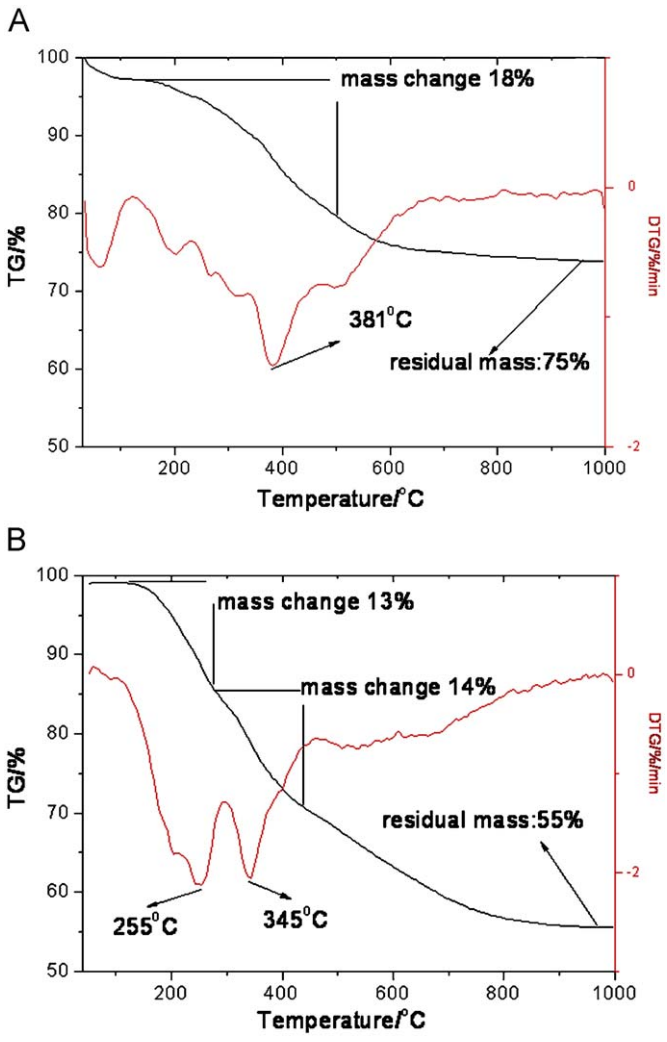

Fig. 8. Thermogravimetry (TG) data for Eu(DBMSi-SBA-15)$_3$phen (A) and Eu(-DBMSi)$_3$ phen complex (B).

3.4. Photoluminescence properties

The luminescence properties of the ternary Eu^{3+} complexes functionalized hybrid mesoporous materials Eu(DBMSi-SBA-15)$_3$phen have been measured at room temperature. Fig. 9 shows the excitation and emission spectra for the pure Eu(DBMSi)$_3$phen complex (A) and SBA-15 mesoporous materials covalently bonded with the binary and ternary Eu^{3+} complexes Eu(DBMSi-SBA-15)$_3$ (B) and Eu(DBMSi-SBA-15)$_3$phen (C). The excitation spectra of these materials at room temperature were all obtained by monitoring the strongest emission wavelength of the Eu^{3+} ions at 613 nm. From the Fig. 9A, it can be seen that a broad excitation band ranging from 220 to 450 nm exists in the excitation spectrum of the pure Eu(DBMSi)$_3$phen complex which is assigened to the $\pi \rightarrow \pi^*$ transition of the ligands [31]. Compared with the pure Eu(DBMSi)$_3$phen complex, the excitation band becomes narrower and the maximum excitation wavelength shifts from 393 to 354 nm for Eu(DBMSi-SBA-15)$_3$phen (see Fig. 9C). The blue shift of the excitation bands can be attributed to a hypsochromic effect corresponding to the change in the polarity of the environment surrounding the europium complex, the introduction of Eu^{3+} complex into the mesoporous material SBA-15 [32].

It is observed a clear characteristic Eu^{3+} ion emission from the emission spectra of Eu(DBMSi-SBA-15)$_3$phen in Fig. 9C. The lines are distributed mainly in the 450–700 nm range, which is assigned to the $^5D_0 \rightarrow {}^7F_J$ ($J = 1$–4) transitions at 580, 621, 645, and 678 nm, respectively. The $^5D_0 \rightarrow {}^7F_1$ transition corresponds to a parity-allowed magnetic dipole transition, which is practically independent of the host material, but the $^5D_0 \rightarrow {}^7F_2$ transition is a typical electric dipole transition and strongly varies with the local symmetry of Eu^{3+} ions. Among these transitions, it is obvious that the $^5D_0 \rightarrow {}^7F_2$ transition shows the strongest emission, indicating that the chemical environment around Eu^{3+} ions is in low symmetry [33,34]. In the pure Eu(DBMSi)$_3$phen complex (Fig. 9A), the stark splitting reveals an ordered "crystalline" rare earth ion environment, rather than an amorphous one. Compared with the typical emissions of the central Eu^{3+}, it is obvious that the broad emission band which mainly originated from the emission of the host SBA-15 and the $\pi \rightarrow \pi^*$ relaxation of the free DBM ligand moiety was very weak, indicating the energy that organic ligand absorbed is not completely transfer to the central Eu^{3+} ion.

In addition, the spectra of Eu(DBMSi-SBA-15)$_3$ (B) and Eu(DBMSi-SBA-15)$_3$phen (C) mesoporous materials were also compared. Not only the intensity of the Eu(DBMSi-SBA-15)$_3$ is weaker than that of Eu(DBMSi-SBA-15)$_3$phen but also the emission peak due to the $^5D_0 \rightarrow {}^7F_{3,4}$ cannot be observed. Furthermore, while irradiated with a UV lamp, the resulting Eu(DBMSi-SBA-15)$_3$phen shows a pure red light and much stronger luminescence than Eu(DBMSi-SBA-15)$_3$, which is in agreement with their emission spectra. In conclusion, we can predicted that the luminescence properties of the mesoporous material Eu(DBMSi-SBA-15)$_3$phen was improved because of the introduction of both the ligand (DBM) and the second ligand (phen) in the mesoporous matrix.

3.5. Luminescence decay times (τ) and emission quantum efficiency (η)

The typical decay curve of the Eu^{3+} hybrid materials were measured and they can be described as a single exponential ($\mathrm{Ln}(S(t)/S0) = -k1t = -t/\tau$), indicating that all Eu^{3+} ions occupy the same average coordination environment. The resulting life-time data (shown in Table 2) appears that the lifetimes of hybrid

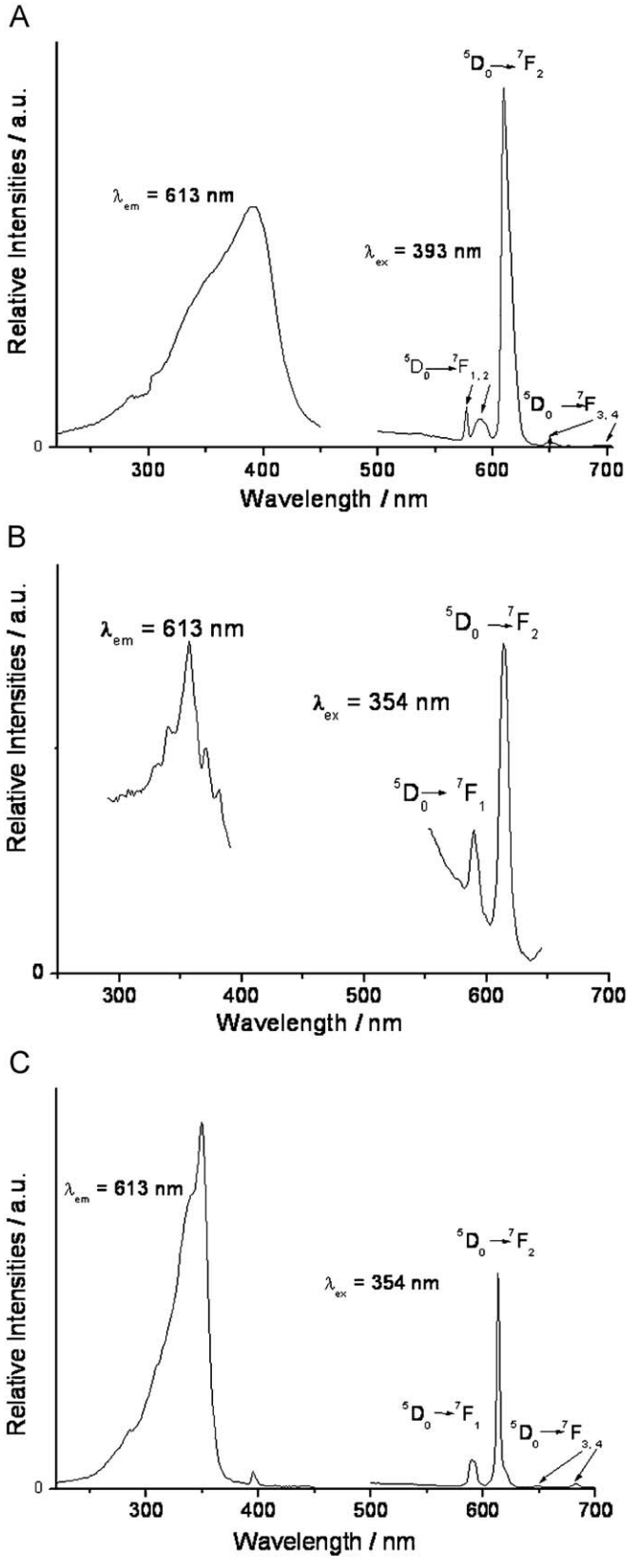

Fig. 9. The excitation and emission spectra for the pure Eu(DBMSi)$_3$phen complex (A), Eu(DBMSi-SBA-15)$_3$ (B), and Eu(DBMSi-SBA-15)$_3$phen (C).

materials are longer than that of pure Eu(DBM)$_3$phen complex, suggesting that the luminescence stability of the pure complex was enhanced after covalently bonded to the mesoporous matrix.

Table 2
Photoluminescent data of Eu(DBMSi)$_3$phen and Eu(DBMSi-SBA-15)$_3$phen.

	Eu (DBMSi)$_3$phen	Eu (DBMSi-SBA-15)$_3$phen
υ_{00} (cm^{-1})	17334	
υ_{01} (cm^{-1})	16954	16929
υ_{02} (cm^{-1})	16398	16289
υ_{03} (cm^{-1})	15356	15408
υ_{04} (cm^{-1})	14382	14649
I_{00}	49.7	
I_{01}	35.7	31.8
I_{02}	448.6	242.6
I_{03}	4.5	4.9
I_{04}	4.5	6.8
A_{00} (s^{-1})	68.1	
A_{01} (s^{-1})	50	50
A_{02} (s^{-1})	649.6	396.4
A_{03} (s^{-1})	6.9	8.5
A_{04} (s^{-1})	6.9	12.4
τ (ms)	0.25	0.7
A_{nrad} (s^{-1})	781.5	467.3
η (%)	20.1	32.7

According to the emission spectrum and the lifetime of the Eu^{3+} first excited level (τ, $^5D_0$), the emission quantum efficiency (η) of the $^5D_0$ Eu^{3+} excited state can be determined. Assuming that only nonradiative and radiative processes are essentially involved in the depopulation of the $^5D_0$ state, η can be defined as follows [35]:

$$n = \frac{A_r}{A_r + A_{nr}} \tag{1}$$

where A_r and A_{nr} are radiative and nonradiative transition rates, respectively. A_r can also be obtained by summing over the radiative rates A_{0J} for each $^5D_0 \rightarrow {}^7F_J$ ($J = 0$–4) transitions of Eu^{3+}

$$A_r = \sum A_{0J} = A_{00} + A_{01} + A_{02} + A_{03} + A_{04} \tag{2}$$

The branching ratio for the $^5D_0 \rightarrow {}^7F_{5,6}$ transitions can be neglected as they are not detected experimentally, whose influence can be ignored in the depopulation of the $^5D_0$ excited state. Since $^5D_0 \rightarrow {}^7F_1$ belongs to the isolated magnetic dipole transition, it is practically independent of the chemical environments around the Eu^{3+} ion, and thus can be considered as an internal reference for the whole spectrum, the experimental coefficients of spontaneous emission, A_{0J} can be calculated according to the equation [36–38]

$$A_{0J} = A_{01}(I_{0J}/I_{01})(\upsilon_{01}/\upsilon_{0J}) \tag{3}$$

Here, A_{0J} is the experimental coefficients of spontaneous emission. A_{01} is the Einstein's coefficient of spontaneous emission between the $^5D_0$ and $^7F_1$ energy levels. In vacuum, A_{01} as a value of 14.65 s^{-1}, when an average index of refraction n equal to 1.506 was considered, the value of A_{01} can be determined to be 50 s^{-1} approximately ($A_{01} = n^3 A_{01\,(vac)}$) [39]. I_{01} and I_{0J} are the integrated intensities of the $^5D_0 \rightarrow {}^7F_1$ and $^5D_0 \rightarrow {}^7F_J$ transitions ($J = 0$–4) with υ_{01} and υ_{0J} ($\upsilon_{0J} = 1/\lambda_J$) energy centers, respectively. υ_{0J} refers to the energy barrier and can be determined from the emission bands of $Eu^{3+}s$ $^5D_0 \rightarrow {}^7F_J$ emission transitions. The emission intensity, I, taken as integrated intensity S of the $^5D_0 \rightarrow {}^7F_{0-4}$ emission curves, can be defined as below:

$$I_{i-j} = \hbar\omega_{i-j}A_{i-j}N_i \approx S_{i-j} \tag{4}$$

where i and j are the initial ($^5D_0$) and final levels ($^7F_{0-4}$), respectively, ω_{i-j} is the transition energy, A_{i-j} is the Einstein's coefficient of spontaneous emission, and N_i is the population of the $^5D_0$ emitting level. The value of $A_{01} \approx 50\,s^{-1}$ and the lifetime (τ), radiative (A_r), and nonradiative (A_{nr}) transition rates are related through the following equation:

$$A_{tot} = 1/\tau = A_r + A_{nr} \tag{5}$$

On the basis of the above discussion, the quantum efficiencies of the materials can be determined, as shown in Table 2. From the equation of η, it can be seen the value η mainly depends on the values of lifetimes and I_{02}/I_{01}. As can be seen from Table 2, the quantum efficiencies of Eu(DBMSi-SBA-15)$_3$phen ($\eta = 32.7\%$) is higher than that of pure Eu(DBMSi)$_3$phen ($\eta = 20.1\%$), which can be ascribe to the substitution of the silanol with covalently bonded DBM groups in the pore channel of mesoporous SBA-15, resulted in the decrease in the level of nonradiative multiphonon relaxation by coupling to –OH vibrations and nonradiative transition rate. This clearly demonstrates the modifications in the Eu^{3+} ion local environment as Eu(DBMSi)$_3$phen is covalently bonded to the mesoporous SBA-15. The results described above further confirm that Eu(DBMSi)$_3$phen is successfully covalently bonded to the SBA-15 network.

4. Conclusion

In summary, we successfully linked the Eu^{3+} complexes to the ordered SBA-15 mesoporous host by the modification of 1,3-diphenyl-1,3-propanepione with 3-(triethoxysilyl)-propyl isocyanate using a co-condensation method. The synthesis of DBMSi-SBA-15 provides a convenient approach of tailoring the surface properties of mesoporous silicates by organic functionalization, and the resulting materials all retain the ordered mesoporous structures. The efficient intramolecular energy transfers from the modified ligand (DBM-Si) to the central Eu^{3+} ions lead to the characteristic luminescence of the corresponding Eu^{3+} in Eu(DBMSi-SBA-15)$_3$phen mesoporous materials. Meantime, the luminescence intensity, the lifetimes, the luminescence quantum efficiency and the thermal stability have also been improved after the ternary complex Eu(DBMSi)$_3$phen covalently bonded to the SBA-15 silicon networks. In conclusion, the method of covalently bonding organometallic complexes to the silica backbone owns more advantages than the conventional method.

Acknowledgments

This work was supported by the National Natural Science Foundation of China (20671072) and Program for New Century Excellent Talents in University (NCET 2008).

References

[1] S. Sato, M. Wada, Bull. Chem. Soc. Jpn. 43 (1970) 1955–1962.
[2] G.F. De Sa, O.L. Malta, C. De Mello Donega, A.M. Simas, R.L. Longo, P.A. Sata-Cruz, E.F. Da Silva, J. Coord. Chem. Rev. 196 (2000) 165–196.
[3] M.D. McGehee, T.B. Bergstedt, C. Zhang, A.P. Saab, M.B. O'Regan, G.C. Bazan, V.I. Srdanov, A.J. Heeger, Adv. Mater. 11 (1999) 1349–1354.
[4] W. Hu, M. Matsumura, M. Wang, L. Jin, Appl. Phys. Lett. 77 (2000) 26–28.
[5] Y.X. Zheng, L.S. Fu, Y.H. Zhou, J.B. Yu, Y. Yu, S.B. Wang, H.J. Zhang, J. Mater. Chem. 12 (2002) 919–923.
[6] O.A. Serra, I.L.V. Rosa, C.L. Medeiros, M. Elizabete, D. Zaniquelli, J. Lumin. 60–61 (1994) 112–114.
[7] L.R. Matthews, E.T. Knobbe, Chem. Mater. 5 (1993) 1697–1700.
[8] B. Yan, J.Y. You, J. Mater. Proc. Technol. 170 (2005) 363–366.
[9] P.A. Tanner, B. Yan, H.J. Zhang, J. Mater. Sci. 35 (2000) 4325–4329.
[10] Q.M. Wang, B. Yan, J. Mater. Chem. 14 (2004) 2450–2455.
[11] Q.M. Wang, B. Yan, J. Photochem. Photobiol. A Chem. 177 (2006) 1–5.
[12] B. Yan, Q.M. Wang, J. Photochem. Photobiol. A Chem. 197 (2008) 213–219.
[13] M.C. Goncalves, V.D. Bermudez, R.A. Sá Ferreira, L.D. Carlos, D. Ostroviskii, J. Rocha, Chem. Mater. 16 (2004) 2530–2543.
[14] P. Lenaerts, A. Storms, J. Mullens, J. Dhaen, C. Gorller-Walrand, K. Binnemans, K. Driesen, Chem. Mater. 17 (2005) 5194–5201.
[15] M.H. Bartl, B.J. Scott, H.C. Huang, G. Wirnsberger, A. Popitsch, B.F. Chmelka, G.D. Stucky, Chem. Commun. (2002) 2474–2475.
[16] B. Yan, H.F. Lu, Inorg. Chem. 47 (2008) 5601–5611.
[17] J.L. Liu, B. Yan, J. Phys. Chem. B 112 (2008) 10898–10907.
[18] J.L. Liu, B. Yan, J. Phys. Chem. C 112 (2008) 14168–14178.
[19] A. Fernandes, J. Dexpert-Ghys, A. Gleizes, A. Galarneau, D. Brunel, Micropor. Mesopor. Mater. 83 (2005) 35.
[20] Q.H. Xu, L.S. Li, X.S. Liu, R.R. Xu, Chem. Mater. 14 (2002) 549–555.
[21] Q.G. Meng, P. Boutinaud, A.C. Franville, H.J. Zhang, R. Mahiou, Micropor. Mesopor. Mater. 65 (2003) 127–136.
[22] Y. Li, B. Yan, J. Solid State. Chem. 181 (2008) 1032–1039.
[23] D.Y. Zhao, J.Y. Sun, Q.Z. Li, G.D. Stucky, Chem. Mater. 12 (2000) 275–279.
[24] S. Madhugiri, A. Dalton, J. Gutierrez, J.P. Ferraris, K.J. Balkus, J. Am. Chem. Soc. 125 (2003) 14531–14538.
[25] B.J. Scott, G. Wirnsberger, G.D. Stucky, Chem. Mater. 13 (2001) 3140–3150.
[26] D.Y. Zhao, Q.S. Huo, J.L. Feng, B.F. Chmelka, G.D. Stucky, J. Am. Chem. Soc. 120 (1998) 6024–6036.
[27] L.N. Sun, J.B. Yu, H.J. Zhang, Q.G. Meng, E. Ma, C.Y. Peng, K.Y. Yang, Micropor. Mesopor. Mater. 98 (2007) 156–165.
[28] W.H. Zhang, X.B. Lu, J.H. Xiu, Z.L. Hua, L.X. Zhang, M. Robertson, J.L. Shi, D.S. Yan, J.D. Holmes, Adv. Funct. Mater. 14 (2004) 544–552.
[29] C.Y. Peng, H.J. Zhang, Q.G. Meng, H.R. Li, J.B. Yu, F.J. Guo, L.N. Sun, Inorg. Chem. Commun. 8 (2005) 440–442.
[30] M.V. Landau, S.P. Parkey, M. Herskowitz, O. Regev, S. Pevzner, T. Sen, Z. Luz, Micropor. Mesopor. Mater. 33 (1999) 149–163.
[31] H.H. Li, S. Inoue, K. Machida, G. Adachi, Chem. Mater. 11 (1999) 3171–3176.
[32] B. Yan, B. Zhou, J. Photochem. Photobiol. A Chem. 195 (2003) 314–322.
[33] P. Miranda Jr., J. Zukerman-Schpector, P.C. Isolani, G. Vicentini, L.B. Zinner, J. Alloys Compds. 344 (2002) 141–144.
[34] X.M. Guo, L.S. Fu, H.J. Zhang, L.D. Carlos, C.Y. Peng, J.F. Guo, J.B. Yu, R.P. Deng, L.N. Sun, N.J. Chem. 29 (2005) 1351–1358.
[35] P.C.R. Soares-Santos, H.I.S. Nogueira, V. Félix, M.G.B. Drew, R.A. Sá Ferreira, L.D. Carlos, T. Trindade, Chem. Mater. 15 (2003) 100–108.
[36] E.S. Teotonio, J.G.P. Espínola, H.F. Brito, O.L. Malta, S.F. Oliveria, D.L.A. de Foria, C.M.S. Izumi, Polyhedron 21 (2002) 1837–1845.
[37] L.D. Carlos, Y. Messaddeq, H.F. Brito, R.A. Sá Ferreira, V. de Zea Bermudez, S.J.L. Ribeiro, Adv. Mater. 12 (2000) 594–598.
[38] R.A. Sá Ferreira, L.D. Carlos, R.R. Gonçalves, S.J.L. Ribeiro, V. de Zea Bermudez, Chem. Mater. 13 (2001) 2991–2998.
[39] M.H.V. Werts, R.T.F. Jukes, J.W. Verhoeven, Phys. Chem. Chem. Phys. 4 (2002) 1542–1548.